

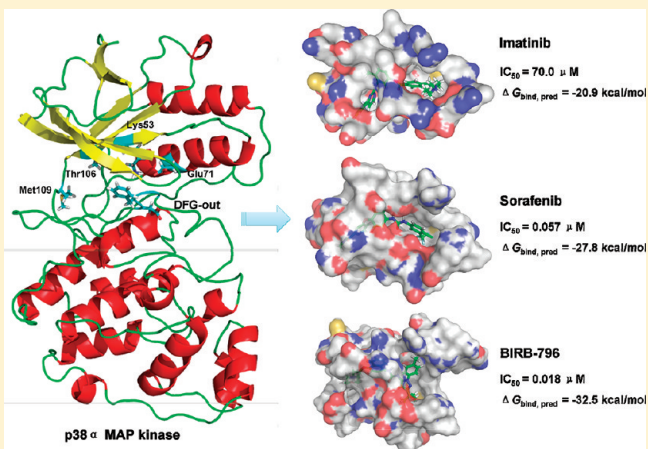
Molecular Dynamics Simulation and Free Energy Calculation Studies of the Binding Mechanism of Allosteric Inhibitors with p38 α MAP Kinase

Ying Yang,[†] Yulin Shen,^{||} Huanxiang Liu,[‡] and Xiaojun Yao*,^{*,†,§}

[†]State Key Laboratory of Applied Organic Chemistry and Department of Chemistry, [‡]School of Pharmacy, and [§]Key Laboratory of Preclinical Study for New Drugs of Gansu Province, Lanzhou University, Lanzhou 730000, China

^{||}Gansu Computing Center, Lanzhou 730030, China

ABSTRACT: p38 MAP kinase is a promising target for anti-inflammatory treatment. The classical kinase inhibitors imatinib and sorafenib as well as BI-1 and BIRB-796 were reported to bind in the DFG-out form of human p38 α , known as type II or allosteric kinase inhibitors. Although DFG-out conformation has attracted great interest in the design of type II kinase inhibitors, the structural requirements for binding and mechanism of stabilization of DFG-out conformation remain unclear. As allosteric inhibition is important to the selectivity of kinase inhibitor, herein the binding modes of imatinib, sorafenib, BI-1 and BIRB-796 to p38 α were investigated by molecular dynamics simulation. Binding free energies were calculated by molecular mechanics/Poisson–Boltzmann surface area method. The predicted binding affinities can give a good explanation of the activity difference of the studied inhibitors. Furthermore, binding free energies decomposition analysis and further structural analysis indicate that the dominating effect of van der Waals interaction drives the binding process, and key residues, such as Lys53, Gly71, Leu75, Ile84, Thr106, Met109, Leu167, Asp168, and Phe169, play important roles by forming hydrogen bond, salt bridge, and hydrophobic interactions with the DFG-out conformation of p38 α . Finally, we also conducted a detailed analysis of BI-1, imatinib, and sorafenib binding to p38 α in comparison with BIRB-796 exploited for gaining potency as well as selectivity of p38 inhibitors. These results are expected to be useful for future rational design of novel type II p38 inhibitors.



INTRODUCTION

The p38 MAP kinase signaling pathway is activated in response to cell stress and induces production of proinflammatory cytokines.¹ Inhibition of this pathway has been demonstrated to reduce inflammation. The p38 kinase family has four members: p38 α , β , γ , and δ . The major isoform p38 α is the main transducer of the inflammatory response and has been a target for anti-inflammatory therapy.^{2–4} Several p38 α inhibitors are in clinical trials for the treatment of chronic obstructive pulmonary disease, psoriasis, and rheumatoid arthritis.^{5–7}

Most kinase inhibitors are ATP competitive, binding exclusively within the ATP binding site of the active DFG-in kinase conformation, so-called type I inhibitors. However, the highly conserved kinase catalytic domain and the similar ATP binding sites make the design of selective type I inhibitors particularly challenging. Utilizing the allosteric pocket with much less conservation, a second class of inhibitors by stabilizing inactive DFG-out kinase conformations has been developed to achieve much better selectivity, known as type II inhibitors.⁸ Therefore, DFG-out conformation has gained great interest in discovery and development

of type II kinase inhibitors for the past few years.^{8–19} Anticancer drugs imatinib (gleevec)^{20,21} and sorafenib (nexavar)²² targeting c-Abl and B-Raf kinases are successful cases of type II inhibitors. BI-1 is a p38 α inhibitor with modest activity and has been refined to BIRB-796 as a highly potent p38 α inhibitor reaching clinical phase II trials for anti-inflammatory therapy.^{16,23,24} The chemical structures and experimental activity against p38 α of the four inhibitors are shown in Figure 1. Recently, the reported X-ray crystal structures indicate these drugs have a shared feature that they bind to the DFG-out forms of their kinase targets.^{12,16,25}

Since 1996, an immense number of p38 inhibitors have been published,^{3,6,7,26,27} and subsequently many efforts have been dedicated to investigate lead discovery strategies targeting p38 MAP kinase. Computational studies on this area have received much attention and wide applications in recent years.^{28–42} Among a variety of approaches in structure-based drug design

Received: April 10, 2011

Published: November 18, 2011

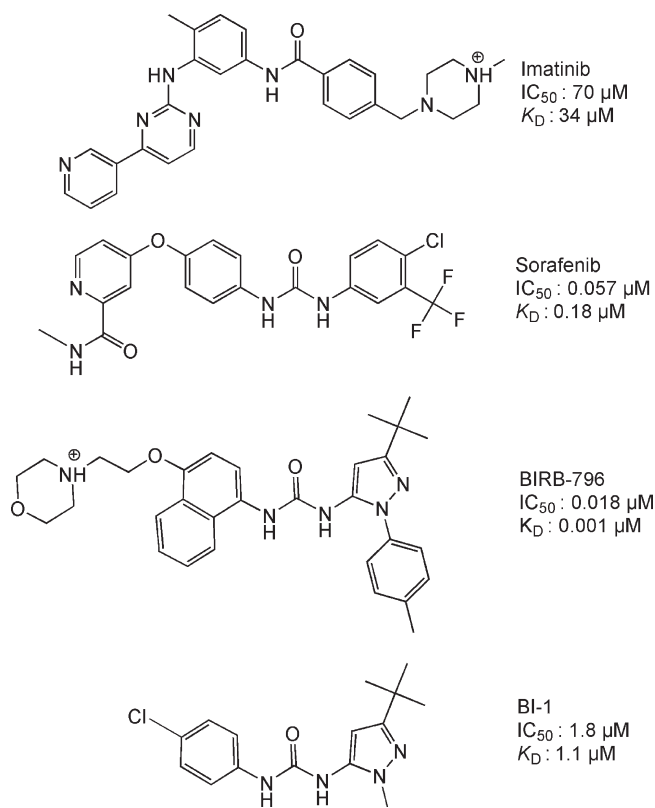


Figure 1. Structures of imatinib, sorafenib, BI-1, and BIRB-796.

fields, molecular dynamics (MD) simulation combined with free energy calculation method has become a powerful tool as it can provide detailed information about the protein–ligand interactions and consider treatments of solvent environment and protein flexibility.⁴³ Due to their success in rapid, accurate, and effective prediction of ligand affinity, the popular molecular mechanics Poisson–Boltzmann surface area (MM-PBSA)⁴⁴ and molecular mechanics/generalized Born surface area (MM-GBSA)⁴⁵ methods have been successfully applied to the study of a variety of systems, such as protein and nucleic acid systems.^{46–64}

To improve our understanding of the structural determinants for type II kinase inhibitors binding and stabilizing the DFG-out conformation, a combined computational approach by MD simulations, MM-PBSA free energy calculations, and MM-GBSA free energy decomposition analysis was performed to imatinib, sorafenib, BI-1 and BIRB-796 with p38 α in the present study. We aimed to investigate the interaction features between p38 α and these inhibitors based on the dynamic structural information from MD and understand the specificity of type II inhibitors by analyzing detailed interaction contributions to binding free energy of the p38 α complexes both energetically and structurally. We also expect that this study will be helpful for the rational design of novel, potent, and selective p38 MAP kinase inhibitors.

MATERIALS AND METHODS

Initial Structure Preparation. The atomic coordinates of the recently obtained crystal structures for BI-1, BIRB-796, imatinib and sorafenib in complexes with p38 α were retrieved from the protein data bank (PDB entries: 1KV1,¹⁶ 1KV2,¹⁶ 3HEC,²⁵ 3HEG,²⁵ and 3GCS,¹² respectively). For sorafenib, there are

two different binding modes in the different crystal structures, here, two kinds of complexes (3HEC and 3GCS) were used for the study of binding mechanism to give a fair assessment. The cocrystal inhibitor and waters were kept. The loop region encompassing residues 171–185 in p38 α not solved in the crystal structures was modeled and refined using the loop building tool in Discovery Studio 2.5.⁶⁵ And then the structures were prepared by Protein Preparation Wizard from Schrodinger Suite 2009,^{66–68} including adding hydrogen atoms, assigning partial charges and protonation states, and carrying out energy minimization with a small number of steps to relax amino residue side chains in vacuum.

The treated structures were used as the initial structures of MD simulation. The partial atomic charges for the ligand atoms were calculated using the restrained electrostatic potential (RESP) protocol after structure optimization and electrostatic potential calculations with a level of quantum mechanical treatment of the ligand using the Q-Site program⁶⁹ based on 6-31G*/LACVP* basis set, B3LYP method. The force field parameters for the ligands generated using the Antechamber program were described by the general amber force field (GAFF).⁷⁰ The standard AMBER 03 force field⁷¹ for bio-organic systems was used to describe the protein parameters. Each protein–ligand binding complex was neutralized by adding suitable counterions and was solvated in a truncated octahedron box of TIP3P⁷² water molecules with a margin distance of 10 Å.

MD Simulation. The MD simulations were performed in AMBER 10.0 software package.⁷³ Initially, the solvated systems were minimized by three steps: First, a harmonic constraint potential of 10 kcal/mol·Å² was applied to all atoms. Second, the protein backbone atoms were restrained with a force of 2.0 kcal/mol·Å². Third, all atoms were allowed to move freely. In each step, energy minimization was executed by the steepest descent method for the first 2500 steps and the conjugated gradient method for the subsequent 5000 steps. After minimization, the systems were gradually heated in the NVT ensemble from 0 to 300 K in 100 ps using a Langevin thermostat with a coupling coefficient of 1.0/ps with a force constant 1.0 kcal/mol·Å² on the complex. And then additional two rounds of MD (50 ps each at 300 K) were performed with decreasing restraint weights reduced from 0.5 to 0.1 kcal/mol·Å². Subsequently the systems were again equilibrated for 500 ps by releasing all the restraints. Finally, the actual MD production run of 10 ns in the NPT ensemble for each system was performed at 300 K with Berendsen⁷⁴ temperature coupling and 1 atm with isotropic molecule-based scaling. During the MD simulations, the long-range Coulombic interactions were handled using the particle mesh Ewald (PME) method.⁷⁵ The cutoff distance for the long-range van der Waals (vdW) energy term was set at 10.0 Å. Periodic boundary conditions were applied to avoid edge effects in all calculations. The SHAKE algorithm⁷⁶ was employed on all atoms covalently bond to hydrogen atoms, allowing for an integration time step of 2 fs. Coordinate trajectories were recorded every 1 ps throughout all equilibration and production runs, and 400 snapshots of the simulated structures within the last 2 ns stable MD trajectory at 5 ps intervals were extracted to perform the following binding free energy calculations.

Binding Free Energy Calculations. The binding free energies (ΔG_{bind}) of the inhibitors with p38 α kinase were calculated by using MM-PBSA procedure in AMBER10.⁴⁴ Average 400 snapshots were extracted from the last 2 ns MD trajectory for the calculations. The binding free energy is computed for

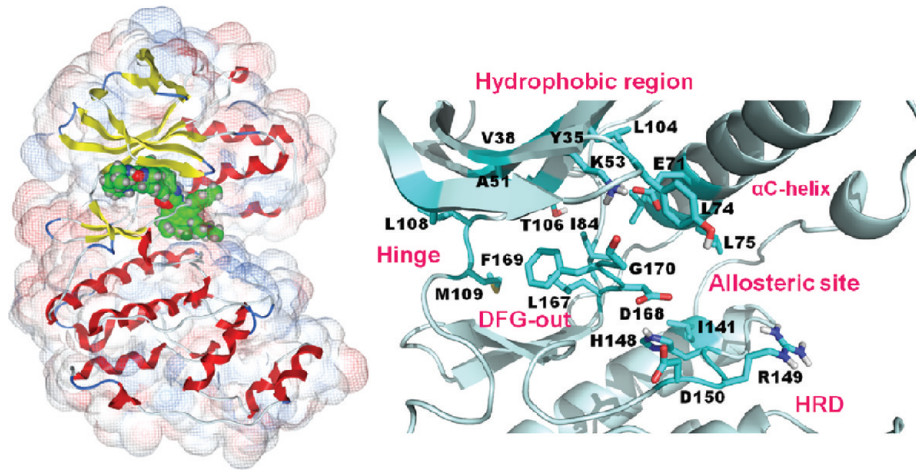


Figure 2. Binding pocket of human p38 α MAP kinase. The spheres represent the inhibitors imatinib, sorafenib, BI-1, and BIRB-796.

each molecular species (complex, protein, and ligand) as the difference:

$$\Delta G_{\text{bind}} = G_{\text{complex}} - (G_{\text{protein}} + G_{\text{ligand}}) \quad (1)$$

Each term can be estimated as follows:

$$\Delta G = \Delta G_{\text{MM}} + \Delta G_{\text{sol}} - T\Delta S \quad (2)$$

where ΔG_{MM} is the molecular mechanics free energy, ΔG_{sol} is the solvation free energy, and $T\Delta S$ represents the entropy term.

The molecular mechanics energy was calculated by the electrostatic and van der Waals interactions:

$$\Delta G_{\text{MM}} = \Delta G_{\text{ele}} + \Delta G_{\text{vdW}} \quad (3)$$

The solvation free energy was composed of the polar and the nonpolar contributions:

$$\Delta G_{\text{sol}} = \Delta G_{\text{ele,sol}} + \Delta G_{\text{nonpol,sol}} \quad (4)$$

where the polar part $\Delta G_{\text{ele,sol}}$ could be calculated by solving the Poisson–Boltzmann (PB) equations⁷⁷ for MM-PBSA method or generalized Born (GB) model⁷⁸ for MM-GBSA. Dielectric constants of 1.0 and 80.0 were used for solute and solvent, respectively. And the parameters used for the GB calculation are developed by Onufriev et al.⁷⁸ (GB^{OBC} , $\text{igb} = 2$).

The nonpolar solvation contribution was determined using the solvent accessible surface area (SASA, \AA^2) with Amber molsurf module, according to:

$$\Delta G_{\text{nonpol,sol}} = \gamma \text{SASA} + b \quad (5)$$

where γ , representing the surface tension, and b , being a constant, were set to 0.0072 kcal/mol· \AA^2 and 0, respectively.

The conformational entropy (translation, rotation, and vibration) upon ligand binding, $T\Delta S$, was calculated using normal-mode analysis with the NMODE program in AMBER10.⁷³ Prior to the normal-mode calculations, each snapshot was minimized for a maximum number of 100 000 cycles using the conjugate gradient method with in the presence of a distance-dependent dielectric of $4r_{ij}$ (r_{ij} is the distance between two atoms) until the root-mean-square of the elements of the gradient vector was less than 1.0×10^{-4} kcal/mol· \AA . Due to the high computational demand of this approach, only 40 snapshots

that were evenly extracted from the last 2 ns MD trajectory were used to calculate the entropic contribution.

Per-Residue Free Energy Decomposition Analysis. To identify the key residues responsible for the binding process of inhibitors, free-energy decomposition to each residue was performed. Given the pairwise nature of the GB equation allowing the decomposition of polar solvation energy ($\Delta G_{\text{ele,sol}}$) into atomic contributions in a straightforward manner, the interaction between inhibitor and each residue was computed using the MM-GBSA decomposition process in AMBER10.^{45,73} The binding interaction of each inhibitor–residue pair includes four terms: van der Waals contribution (ΔG_{vdW}), electrostatic contribution (ΔG_{ele}), polar solvation contribution ($\Delta G_{\text{ele,sol}}$), and nonpolar solvation contribution ($\Delta G_{\text{nonpol,sol}}$):

$$\Delta G_{\text{inhibitor-residue}} = \Delta G_{\text{vdW}} + \Delta G_{\text{ele}} + \Delta G_{\text{ele,sol}} + \Delta G_{\text{nonpol,sol}}$$

where the vdW and electrostatic interactions between inhibitor and per residue of p38 α were computed using the Sander program in AMBER10.⁷³ The polar solvation contribution ($\Delta G_{\text{ele,sol}}$) was calculated by using the generalized Born (GB) model (GB^{OBC} , $\text{igb} = 2$).⁷⁸ The nonpolar contribution of desolvation ($\Delta G_{\text{nonpol,sol}}$) was computed based on SASA. All energy components were calculated using 400 snapshots extracted from the MD trajectory from last 2 ns.

■ RESULTS AND DISCUSSION

Static Structural Analysis of Inhibitor Binding Mode. The X-ray cocrystal complexes of four inhibitors and p38 α MAP kinase reveal that the kinase exists in the DFG-out conformation and four inhibitors share a similar binding mode (Figure 2). The inhibitors were stabilized in a cavity formed by the residues Tyr35, Val38, Ala51, Lys53, Gly71, Leu74, Leu75, Ile84, Leu104, Thr106, Leu108, Met109, Ile141, His148, Arg149, Asp150, Leu167, Asp168, and Phe169. In this active site, the inhibitors form one hydrogen bond with the backbone NH of Met109 in the hinge region and bridging hydrogen bond network between the conserved side-chain carboxyl group of Glu71 in α C-helix and the backbone NH of Asp168 involved in the DFG loop movement. The hydrophobic interactions include two regions: hydrophobic pocket I (HP I) surrounded by the residues Val38,

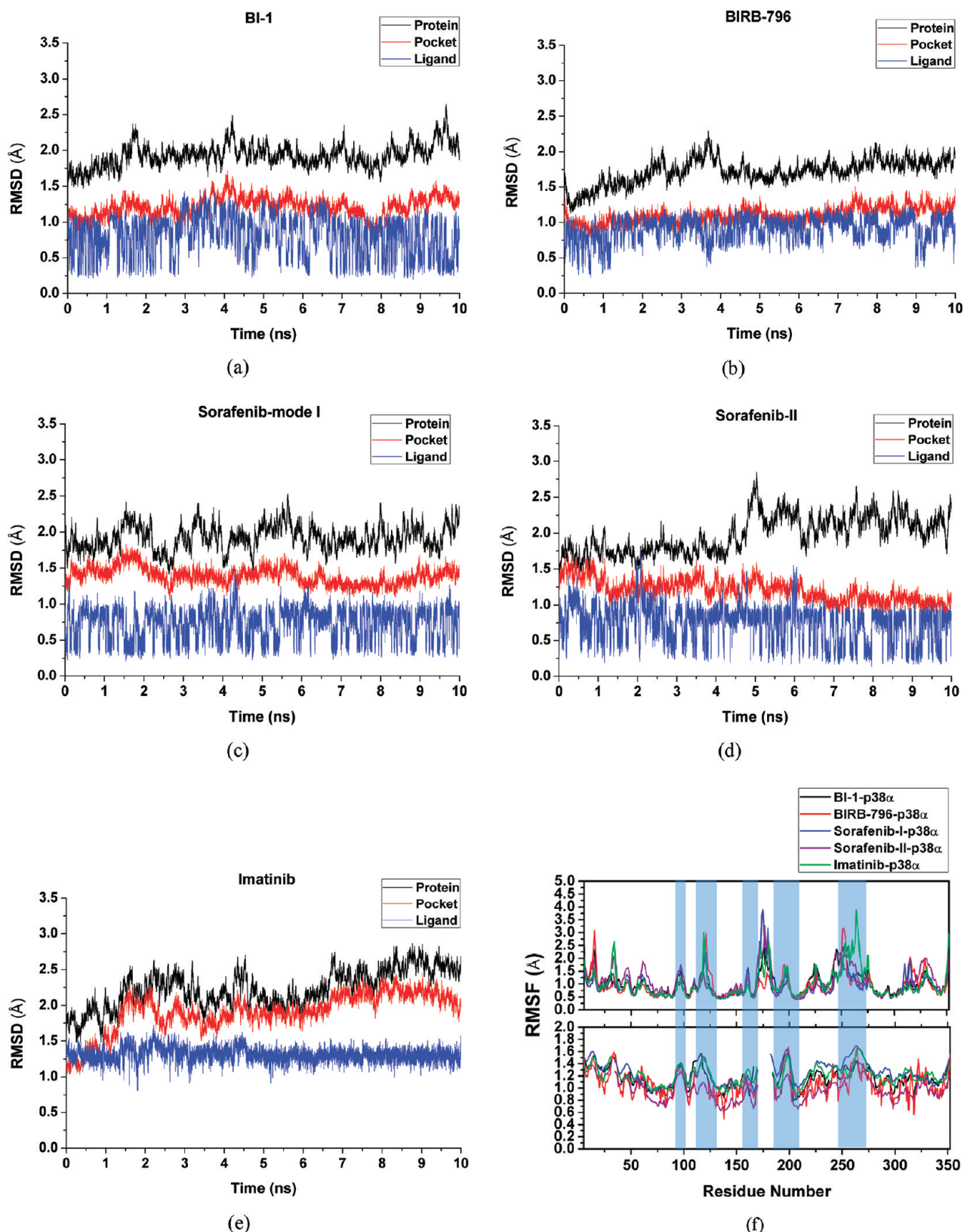


Figure 3. RMSDs of C α atoms of the protein, backbone atoms of binding pocket (within 6.5 Å), and the heavy atoms in the ligand for: (a) BI-1, (b) BIRB-796, (c) sorafenib-I (d), sorafenib-II, and (e) imatinib-bound p38 α complexes as a function of the simulation time. (f) RMSF of each residue of the protein for all five complexes obtained from crystal structure (bottom) and 10 ns MD simulation (top).

Ala51, Lys53, Leu104, Thr106, and Leu108, and hydrophobic pocket II (HP II) surrounded by the residues Leu74, Leu75,

Met78, Val83, Ile84, Ile141, and Ile146. HP I is controlled by the gatekeeper residue Thr106 to access this pocket and close to the

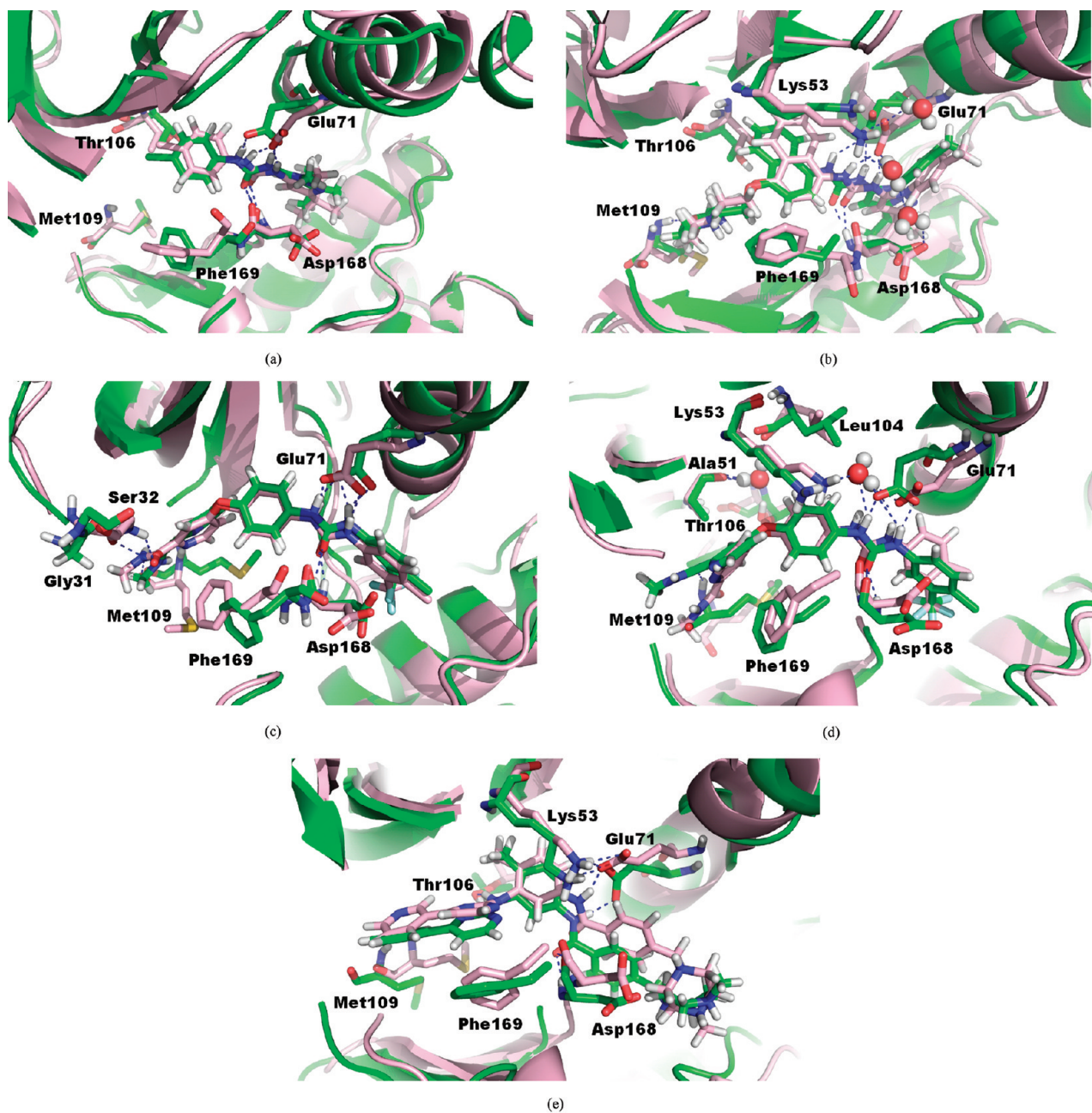


Figure 4. Structure comparison between initial (green) and representative snapshot from MD (pink) of: (a) BI-1, (b) BIRB-796, (c) sorafenib-I, (d) sorafenib-II, and (e) imatinib at the active site of p38 α . Blue dots represent hydrogen bonds.

conserved Lys53. HP II is the so-called allosteric pocket, comprised of two sites related to the inhibitor's selectivity. One site is orientated in the lower position of the allosteric pocket extending to the HRD motif, which is made by Phe169 flipping out of its lipophilic pocket in the movement of DFG loop. The other site in the upper position of the allosteric pocket was found to be occupied by the tolyl ring of BIRB-796 in the crystal structure (PDB: 1KV2), which is less conserved.¹¹ However, sorafenib binds to p38 α in a DFG-out form with two different ligand conformations reported by two different groups.^{12,25} In sorafenib binding mode I (PDB: 3HEG), the pyridine nitrogen forms hydrogen bond with the main chain NH of Met109 in the hinge.²⁵ In sorafenib binding mode II (PDB: 3GCS), the pyridyl

nitrogen is rotated and does not interact with the hinge.¹² Instead, the carbonyl O of the picolinamide forms hydrogen bond with the main chain NH of Met109, and the Met109 side chain is also rotated out of the inhibitor binding site. And detailed structural requirements and interactions with p38 α for allosteric inhibitors will be further investigated and discussed in the following sections.

MD Simulations. Overall Structural Flexibility and Stability. MD simulations for five complexes in explicit aqueous solution were run for duration of 10 ns. To explore the dynamic stability of complexes and to ensure the rationality of the sampling method, root-mean-square deviations (RMSD) from the starting structure were analyzed, as shown in Figure 3. As can be seen in the plots, after 5 ns, the RMSD of each system except imatinib–p38 α complex

Table 1. Hydrogen-Bond Analysis from the Results of MD Simulation

system	donor	acceptor	occupancy (%) ^a	distance (Å) ^b	angle (°) ^c
BI-1-p38 α	ligand HN9	Glu71 OE1	100.0	2.801 (0.001)	17.57 (0.07)
	ligand HN2	Glu71 OE1	100.0	2.795 (0.001)	26.66 (0.08)
	Asp168 NH	ligand O1	93.8	3.059 (0.002)	17.90 (0.10)
	Lys53 HZ	Glu71 OE1	35.6	2.846 (0.001)	26.92 (0.14)
	solvent	Glu71 OE2	35.4	2.786 (0.002)	22.45 (0.14)
BIRB-796-p38 α	ligand HN2	Glu71 OE2	99.9	2.777 (0.001)	18.76 (0.10)
	ligand HN9	Glu71 OE2	97.8	2.976 (0.002)	27.72 (0.14)
	Asp168 NH	ligand O1	97.2	3.017 (0.002)	18.17 (0.12)
	Met109 NH	ligand O47	89.9	3.001 (0.002)	25.16 (0.12)
	Lys53 HZ	Glu71 OE1	98.3	2.776 (0.001)	24.32 (0.12)
	solvent	Lys53 HZ	77.7	2.927 (0.002)	28.03 (0.15)
	solvent	Asp168 O	30.7	2.879 (0.002)	28.60 (0.13)
	solvent	Glu71 OE1	30.7	2.879 (0.003)	28.60 (0.17)
sorafenib-I-p38 α	Asp168 NH	ligand O15	99.3	2.969 (0.002)	19.66 (0.11)
	ligand H5	Glu71 OE1	93.7	2.761 (0.001)	16.73 (0.09)
	ligand HN1	Glu71 OE2	83.2	2.957 (0.002)	19.22 (0.10)
	ligand HN1	Glu71 OE1	78.4	3.164 (0.002)	37.83 (0.10)
	Met109 NH	ligand N26	56.5	3.231 (0.002)	18.52 (0.10)
	Lys53 HZ	Glu71 OE1	85.2	2.774 (0.001)	29.72 (0.13)
sorafenib-II-p38 α	ligand HN1	Glu71 OE2	100.0	2.782 (0.001)	19.19 (0.08)
	ligand HN2	Glu71 OE2	98.6	2.927 (0.001)	33.80 (0.11)
	Asp168 NH	ligand O15	99.6	2.934 (0.002)	20.42 (0.09)
	Met109 NH	ligand O32	97.8	2.986 (0.002)	18.38 (0.10)
	solvent	Ala51 O	93.5	2.805 (0.002)	23.51 (0.13)
	solvent	Leu104 O	89.5	2.886 (0.002)	22.51 (0.12)
	solvent	Lys53 HZ	48.0	2.944 (0.002)	32.59 (0.15)
imatinib-p38 α	solvent	Glu71 OE1	37.1	2.908 (0.003)	28.12 (0.17)
	solvent	Glu71 OE2	35.3	2.810 (0.002)	21.80 (0.14)
	ligand HN2	Glu71 OE1	99.9	2.836 (0.001)	18.16 (0.07)
	Met109 NH	ligand N3	93.8	3.080 (0.002)	21.07 (0.11)
	ligand HN1	Thr106 OG1	39.8	3.248 (0.002)	36.32 (0.11)
	Asp168 NH ^d	ligand O29	28.3	3.272 (0.002)	33.67 (0.13)
Lys53 HZ	Glu71 OE1	97.0	2.773 (0.001)	24.16 (0.12)	
	Glu71 OE2	40.6	3.119 (0.002)	41.65 (0.12)	
	solvent	Glu71 OE2	34.7	2.724 (0.002)	20.21 (0.12)

^a The listed donor and acceptor pairs satisfy the criteria for the hydrogen bond over 30.0% occupancy during the 10 ns of simulation. The occupancy of hydrogen bond between Asp168 NH and ligand O29 in imatinib-p38 α system is less than 30.0%. ^b The average distance with standard error (SE = standard deviation/N^{1/2}) in parentheses between hydrogen-acceptor atom and hydrogen-donor atom in the investigated time period. ^c The average angle with standard error (SE = standard deviation/N^{1/2}) in parentheses for hydrogen bond in the investigated time period.

tends to converge, indicating the systems are stable and equilibrated. The imatinib-p38 α complex shows the highest fluctuations among the five, with average RMSDs of 2.236 and 1.311 Å for protein and ligand, respectively, indicating that imatinib has an unstable binding with p38 α .

Furthermore, analyses of root-mean-square fluctuation (RMSF) versus the residue number for complexes are illustrated in Figure 3f. For comparison, the corresponding values of RMSFs obtained from the experimental B-factors in crystal structures are also shown in Figure 3f (bottom). The experimental B-factors are transformed to the RMSF with the equation $\langle \Delta r_i^2 \rangle = 3Bi/(8\pi^2)$.⁷⁹ RMSF profiles indicate that the residues with higher fluctuation values are those in the flexible loops (light-blue shadows in Figure 3f). Although the residues Leu171-Gly181 in the activation loops were not resolved in the crystal

structures, RMSFs of the neighboring residues to the missing loops show similar trend between MD values and experimental data. The observations are in agreement with the experimental results reflected by the B factors derived from the X-ray crystallographic data, indicating the reasonability of our MD results. Accordingly, the protein structures of all systems share similar RMSF distributions and similar trends of dynamic features. And this suggests all inhibitors have similar interaction mechanism with p38 α . For p38 α bound complexes, it shows relatively rigid in the active site region (residues 35, 38, 51, 53, 71–75, 84, 104–109, 135–141, and 167–169). The fluctuation of the active site for imatinib-p38 α complex is more significant, and BIRB-796-p38 α complex is smallest among the five complexes.

Conformational Changes of the Active Site Region. To further investigate inhibitor-p38 α interactions in the binding

Table 2. Binding Free Energies and Its Components for the Studied Inhibitors with p38 α ^a

ligand-p38 α	BIRB-796	sorafenib-I	sorafenib-II	BI-1	imatinib
ΔG_{vdW}	-75.07 (0.16)	-52.86 (0.15)	-55.64 (0.16)	-42.72 (0.15)	-55.56 (0.18)
ΔG_{ele}	-165.99 (0.42)	-54.64 (0.28)	-41.63 (0.24)	-38.41 (0.33)	-325.73 (0.79)
$\Delta G_{nonpol, sol}$	-9.31 (0.01)	-7.25 (0.01)	-7.50 (0.01)	-5.64 (0.01)	-6.49 (0.01)
$\Delta G_{ele, sol}$ (PB)	194.48 (0.38)	64.63 (0.21)	51.54 (0.19)	44.07 (0.34)	343.13 (0.72)
$\Delta G_{ele, sol}$ (GB)	179.67 (0.37)	57.35 (0.19)	45.61 (0.17)	39.08 (0.28)	344.63 (0.73)
$\Delta H_{(PB)}$	-55.90 (0.23)	-50.12 (0.18)	-53.22 (0.21)	-43.70 (0.19)	-44.64 (0.22)
$\Delta H_{(GB)}$	-70.71 (0.18)	-57.40 (0.16)	-59.15 (0.16)	-48.69 (0.14)	-43.14 (0.17)
$T\Delta S$	-23.32 (0.95)	-22.27 (1.29)	-25.87 (1.31)	-21.61 (1.08)	-23.67 (0.52)
ΔG_{pred} (PB)	-32.58 (1.15)	-27.85 (0.96)	-27.35 (1.43)	-22.09 (1.15)	-20.97 (0.86)
ΔG_{pred} (GB)	-47.39 (1.17)	-35.13 (0.77)	-33.28 (1.42)	-27.08 (1.14)	-19.47 (0.74)
IC_{50} (μM)	0.018	0.057	0.038 ^b	1.8	70
ΔG_{exp}	-10.64	-9.95	-10.20	-7.89	-5.71

^a Mean energies are in kcal/mol, with corresponding standard errors (SE = standard deviation/ $N^{1/2}$)^{48,57,63} in parentheses. ΔH : the enthalpy changes, $\Delta H = \Delta G_{ele} + \Delta G_{vdW} + \Delta G_{nonpol,sol} + \Delta G_{ele,sol}$. $T\Delta S$: the entropy changes. ΔG_{pred} : the calculated binding free energy by MM-PB(GB)SA method. ΔG_{exp} : the experimental binding free energy calculated according to the IC_{50} by $\Delta G \approx -RT \ln IC_{50}$. ^b $IC_{50}(\mu M)$: 0.038 – 3.2; ΔG_{exp} (kcal/mol): -10.20 – -7.55.

process, we compared the representative snapshots taken from last 2 ns MD trajectory with their initial structure before MD. Figure 4 shows the aligned structures at the active site for the five p38-bound complexes. It can be seen that the side-chain carboxyl of Glu71 has a similar trend to rotate 90° in all systems, which results in only one carboxyl O formed hydrogen bond with NH of urea or amide group of inhibitors. However, this trend is not significant in sorafenib-II–p38 α and BI-1–p38 α complexes, for both carboxyl O atoms of Glu71 could still make hydrogen bonds with both urea NH groups of sorafenib and BI-1. Thereby, salt bridge interaction between Glu71 and Lys53 disappeared in sorafenib-II–p38 α complex and was weak in BI-1–p38 α complex (Table 1). The side-chain phenyl of Phe169 turns toward sorafenib-I–p38 α and BI-1–p38 α complexes. Three water molecules were obtained from MD to bridge hydrogen bonds among Lys53, Glu71, and Asp168 in BIRB-796–p38 α complex. Imatinib undergoes a large movement after MD, with an average RMSD of 1.311 Å, which causes the side chains of Met109, Glu71, and Asp168 to flip (Figure 4e). In sorafenib-II–p38 α , ring groups in both sides of sorafenib rotate inward, and two water molecules are stably bridging the hydrogen-bond networks among Ala51, Leu104, Thr106, Lys53, and Glu71 (Figure 4d).

The hydrogen bond plays an important role in inhibitor binding to kinase. For the five protein–inhibitor systems, the hydrogen-bond interactions with key residues in the binding pocket are listed in Table 1 and shown in Figure 4. Among the four allosteric inhibitors, they formed stable hydrogen bonds with Glu71 and Asp168, except for imatinib only with Asp168 (28% occupancy). BIRB-796, sorafenib-II, and imatinib formed stable hydrogen bonds with residue Met 109 in the hinge region. In sorafenib-II–p38 α , water molecules form hydrogen bonds with Ala51 and Leu104, with high occupancies of 93% and 89%, respectively. And solvent water formed hydrogen bond with Lys53, Glu71, and Asp168 just occasionally in the five systems.

Interaction Mechanism Based on the Binding Free Energy Calculation. The binding free energies of all five systems were calculated by using *mm_pbsa* program in AMBER. In Table 2, we present the predicted and experimental relative binding affinities, together with their respective enthalpic and entropic contributions. As can be seen, the ranking of the predicted binding free energies are in good agreement with the experimental

activity.^{12,25} It needs to be noted that the binding free energies calculated with MM-PBSA and MM-GBSA do not reproduce the absolute experimental values accurately, but they have been shown to correlate with the experiment values well.^{12,16,25} Given the more underestimation of MM-GBSA calculation, compared with that of MM-PBSA, our discussion about binding free energy is mainly based on the results of MM-PBSA. From the results, our prediction of binding free energy shows that the differences between BIRB-796 and the other inhibitors are statistically significant (the *t* distribution value is ~2 at 95% confidence level, and the difference must be larger than twice standard error (SE)⁶³ to be statistically significant).

Besides ranking the binding free energies correctly, another advantage of MM-PBSA and MM-GBSA is that it allows us to decompose the total binding free energy into individual components, thereby enabling us to understand the complex binding process in detail. In the five studied protein–inhibitor complexes, the van der Waals interactions and the nonpolar solvation energies responsible for the burial of inhibitor's hydrophobic groups upon binding are the basis for favorable binding free energies. The favorable Coulomb interactions within the protein–inhibitor complexes are counteracted by the unfavorable electrostatics of desolvation. The resulting balance of the electrostatic interaction contributions in vacuum and solvent, namely $\Delta G_{ele} + \Delta G_{ele, sol}$ is unfavorable to binding in all the five systems.

Identification of the Key Residues Responsible for the Binding of Inhibitor. To identify the key residues related with the binding process, the binding free energy between the protein and inhibitor was decomposed into the contribution of each residue. The interaction information in the five inhibitor–p38 α complexes is shown in Figure 5 and the contributions of key residues for five complexes are compared in Figure 6. As can be seen from Figure 5, the major favorable energy contributions originate predominantly from the residues Glu71, Leu75, Ile84, Leu167, and Asp168 of p38 α in common in all five complexes. Special attention had been paid to those residues with relatively large difference of the contribution to binding free energies. For example, with a level of the estimated standard errors smaller than ~0.03 kcal/mol and the differences larger than ~0.10 kcal/mol, the residues Leu75, Ile84, Thr106, and Leu167 have stronger interactions with BIRB-796 compared with the others,

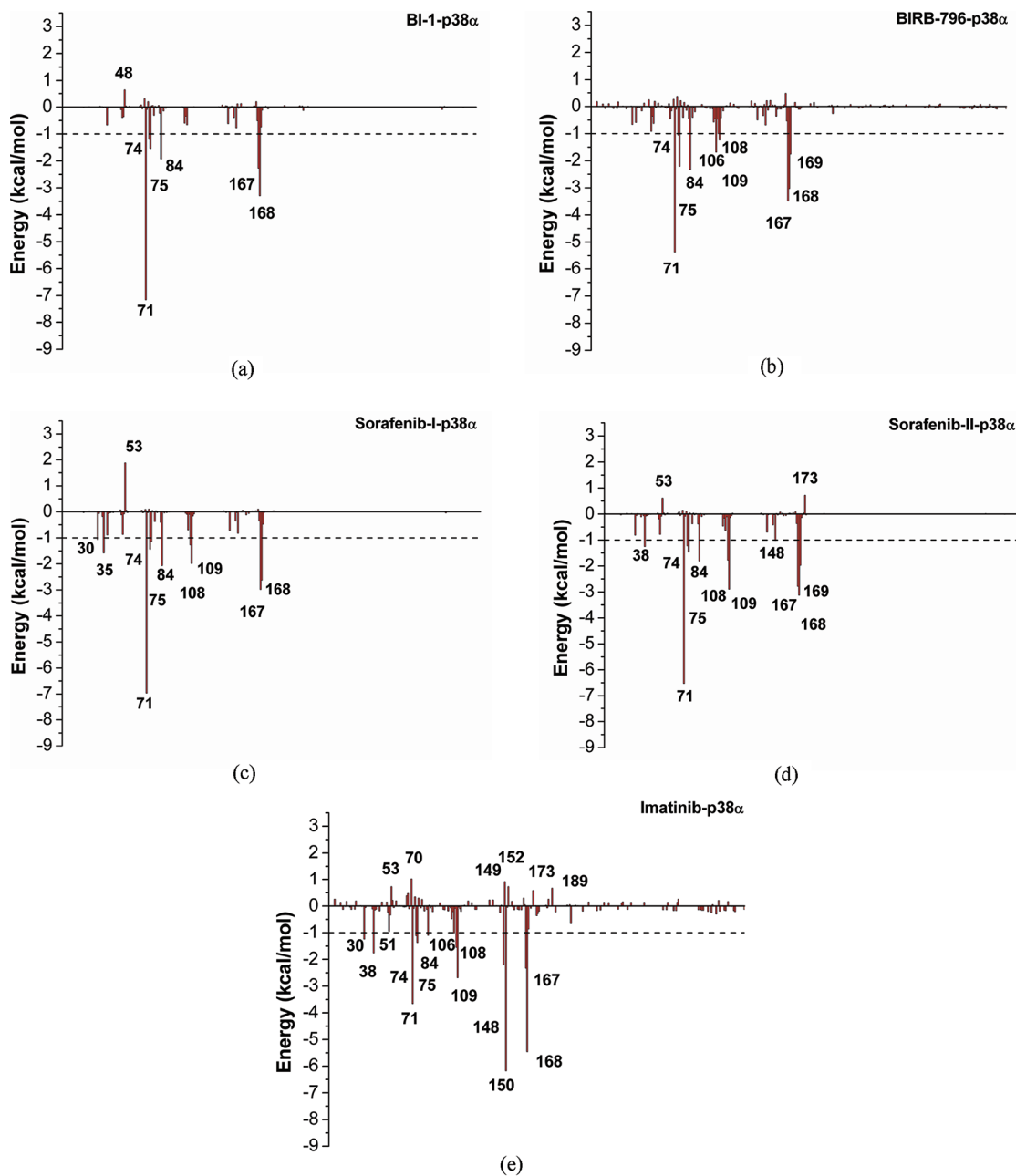


Figure 5. Inhibitor–residue interaction spectra of: (a) BI-1, (b) BIRB-796, (c) sorafenib-I, (d) sorafenib-II, and (e) imatinib.

while the residues Val38, His148, and Asp150 interact with imatinib differently from the other inhibitors. The residue Phe169 contributes more than twice to sorafenib-II (-1.98 ± 0.02 kcal/mol) and BIRB-796 (-1.76 ± 0.02 kcal/mol) compared to imatinib (-0.86 ± 0.02 kcal/mol), BI-1 (-0.74 ± 0.02 kcal/mol), and sorafenib-I (-0.48 ± 0.02 kcal/mol). As can be seen in Figure 6, the contributions of van der Waals and nonpolar solvation energies of residues Lys53, Glu71, Leu75, Ile84, Thr106, Leu167, and Asp168 (with a level of the estimated standard errors smaller than ~ 0.04 kcal/mol and the differences larger than ~ 0.15 kcal/mol) were mainly responsible for the differences between BIRB-796 and the others. And the total electrostatic energies of residues His148, Asp150, and Asp168 (with a level of the estimated standard errors smaller than ~ 0.2 kcal/mol and the differences larger than ~ 1.8 kcal/mol)

participate in yielding energetic differences for imatinib, compared with the others. From these results, we could conclude that hydrogen bond and hydrophobic interactions played an important role in the binding affinity with residues Glu71, Leu75, Ile84, Thr106, Leu167, Asp168, and Phe169.

Furthermore, it is essential for further rational design of more potent selective allosteric inhibitors targeting the DFG-out form of kinase to understand the structural requirements of the ligand to enhance the binding affinity through a detailed comparison between these representative type II inhibitors. For this reason, we will focus on the comparison in interaction features of BIRB-796, as the most potent inhibitor, with other inhibitors.

Comparison between the Binding Mode of BIRB-796 and BI-1 with p38 α . Three major changes in structure lead to the increased activity of BIRB-796 compared to that of BI-1. They

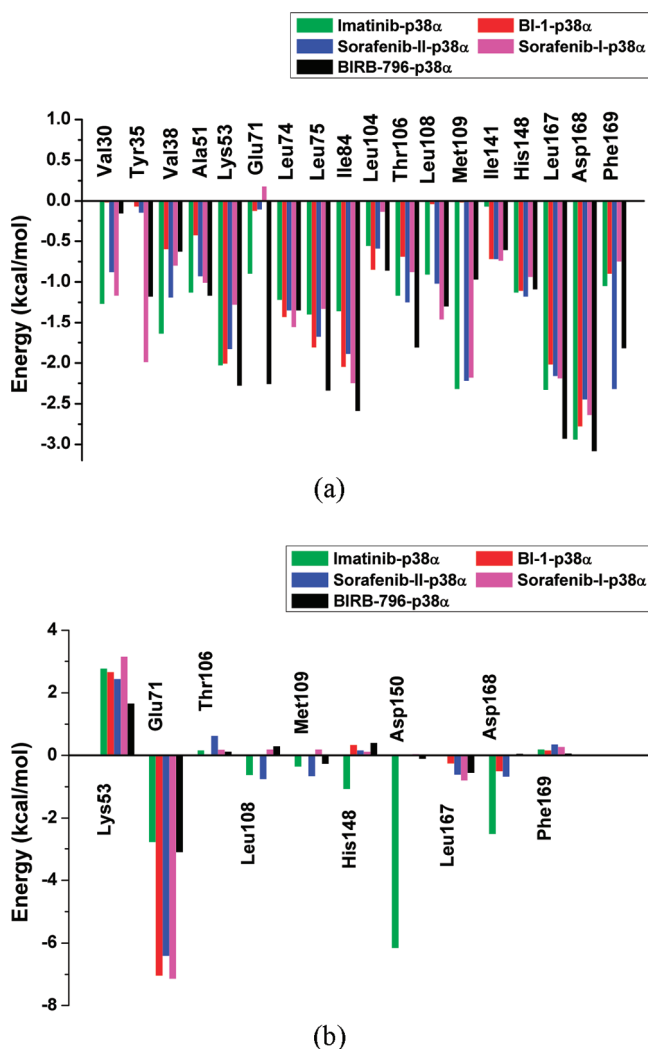


Figure 6. Comparison of per-residue energy decomposition for key residues for five systems: (a) the sum of vdW and nonpolar solvation energy, $\Delta G_{vdW} + \Delta G_{nonpol,sol}$ and (b) the sum of electrostatic and polar solvation energy, $\Delta G_{ele} + \Delta G_{ele,sol}$.

are the replacements of the methyl substituent on the pyrazole ring with a tolyl group, the chlorophenyl group with the naphthyl moiety and the introduction of an ethoxymorpholine substituent on the naphthyl ring. The predicted binding free energy for BIRB-796 with p38 α is lower than that for BI-1, averagely with the difference of 10 kcal/mol, in accordance with the observed activity.²⁵ In Figure 4, it can be seen that the morpholine group of BIRB-796 forms a stable hydrogen bond with Met109 at the hinge region. This favorable hydrogen-bond interaction is supported by the per-residue energy decomposition, which shows the energy contributions of Met109 are -1.24 ± 0.02 kcal/mol to BIRB-796 and -0.01 ± 0.01 kcal/mol to BI-1. Due to this morpholine group, the hydrophobic interaction of Leu108 with BIRB-796 increased to -1.01 ± 0.02 kcal/mol, whereas the hydrophobic interaction with BI-1 is 0.00 ± 0.01 kcal/mol. The residues Thr106 and Leu167 also contribute energetically more to BIRB-796 than to BI-1. The ventral end of the naphthalene of BIRB-796 forms an edge-to-face interaction with Phe169, leading that the energy contribution of Phe169 to BIRB-796 increased by 1.02 kcal/mol, compared to BI-1. The conserved

Glu71 in helix α C contributes -7.16 ± 0.05 kcal/mol to BI-1 binding including the contribution from total electrostatic energies -7.04 ± 0.19 kcal/mol, sum of van der Waals and nonpolar solvation energies -0.12 ± 0.04 kcal/mol. While in the BIRB-796 binding, Glu71 contributes -5.37 ± 0.03 kcal/mol including total electrostatic energies of -3.11 ± 0.17 kcal/mol, sum of van der Waals and nonpolar solvation energies of -2.26 ± 0.04 kcal/mol. This is due to the fact that the tolyl group of BIRB-796 favorably interacting with hydrophobic portions of the side chain of Glu71. It causes the conformational change in Glu71 so that the urea NH group in BIRB-796 can form a hydrogen bond with only one of carboxyl O of Glu71. And both urea NH group in BI-1 can form hydrogen bond with Glu71 without this hydrophobic interaction. These are supported by hydrogen-bond analysis (Table 1). However, BIRB-796 binds deeply into the active pocket of p38 α , creating favorably hydrophobic interactions with more residues than that with BI-1.

Comparison between the Binding Mode of BIRB-796 and Sorafenib with p38 α . The structural differences are large between the two inhibitors except that sorafenib remains the urea group same to BIRB-796 to form hydrogen bonds with Glu71 and Asp168. Sorafenib was reported to adopt a type II binding mode with the DFG-out conformation of p38 α in two different poses as mentioned early.^{12,25} The halogenated phenyl moiety of sorafenib is equivalent to the *tert*-butyl pyrazole moiety of BIRB-796, residing in the allosteric site. But the residue Glu71 forms a pair of symmetric hydrogen bonds to both urea nitrogens of sorafenib, differently from that of BIRB-796. The components of bind free energy demonstrate that the van der Waals interactions make average ~ 20 kcal/mol differences between the two inhibitors. The per-residue energy contribution shows that the interaction modes are similar, except for Lys53 and Arg173 with unfavorable electrostatic interactions to the binding of sorafenib. Although the pyridine ring of both conformations of sorafenib–p38 α complex is close to the side chain of Phe169 of the DFG-motif, allowing for favorable edge-to-face interactions, the residue Phe169 contributes -0.48 ± 0.02 kcal/mol to mode I and -1.98 ± 0.02 kcal/mol to mode II, differently. It is probably caused by the induced conformational change on the side chain of Met109. This change leads to the steric clash between the phenyl of Phe169 and the methylthio of Met109 in the binding mode I, thereby weakening the interaction of Phe169 with sorafenib-I. Furthermore, in sorafenib-II–p38 α , both co-crystal structure and MD results suggest the phenoxy oxygen accesses the hydroxyl of the gatekeeper residue Thr106 and coordinates a water molecule that can form hydrogen bonds with the backbone carbonyls of Leu104 and Ala51 and hydroxyl of Thr106. This water-mediated hydrogen bond has not been reported in the BIRB-796–p38 α cocrystal structure. And our hydrogen-bond analysis from MD also proves this water-mediated interaction exists in sorafenib-II–p38 α complex, not in the BIRB-796-bound (Table 1).

Comparison between the Binding Mode of BIRB-796 and Imatinib with p38 α . Imatinib was also reported to bind with p38 α in a DFG-out conformation in similar with BIRB-796.²⁵ In the ATP binding site, imatinib interacts with p38 α via two hydrogen bonds to the hinge (Figure 4e), one through the N atom of the pyrimidine and the backbone amide NH of Met109 and the other through the NH linker and hydroxyl of Thr106. The amide and oxygen of imatinib form a hydrogen bond to the carboxylate oxygen of Glu71 and backbone amide of Asp168, respectively. BIRB-796 shares similar binding mode but does not

form hydrogen bond with Thr106. Moreover the piperazine group of imatinib within the protein cavity extends into the solvent. In the cocrystal structure of imatinib–p38 α , a central water molecule coordinates among the pyrimidine nitrogen of the inhibitor, the nitrogen of Lys53, and the Asp168 main chain carbonyl oxygen atom. This is also revealed by the hydrogen-bond analysis of the trajectory in MD simulation. The pyrimidine ring of imatinib has a face-to-face interaction with Phe169, energetically less favorable compared to edge-to-face in BIRB-796/sorafenib (I and II)-bound status. The per-residue energy decomposition shows that Phe169 contributes -0.86 kcal/mol to imatinib, -1.98 kcal/mol to sorafenib-II, and -1.76 kcal/mol to BIRB-796, at a level of the estimated standard errors within 0.02 kcal/mol. These interactions between several type II inhibitors in complex with p38 α presented here may provide further opportunities for the development of inhibitors that not only induce the inactive kinase conformation but also stabilize it by interacting with Phe169 directly within the ATP binding site. However, due to more unfavorable residue interactions and decreasing van der Waals interaction with p38 α , the binding affinity of imatinib is weak. This is in agreement with the experimental activity.²⁵

CONCLUSIONS

In this study, MD simulation and free energy calculation were used to investigate the interactions of allosteric kinase inhibitors BI-1, BIRB-796, sorafenib, and imatinib to human p38 α MAP kinase. The analysis of the components in binding free energy suggests that the major contribution to the binding of p38 α and inhibitors is by the van der Waals energy component, affecting the differences of binding affinity among the four inhibitors. The per-residue energy decomposition demonstrates the favorable and unfavorable interactions of individual residue. In the five inhibitor–p38 α complexes under study, the hydrogen bonds bridging the conserved Glu71 in C-helix and the Asp168 in DFG motif are essential for stabilizing the DFG-out conformation of protein. The interactions with Met109 at the hinge region formed hydrogen bonds, and with Phe169 formed edge-to-face, T-shape for both π -electron systems can enhance inhibitory activity. The hydrogen bonds are not only favorable to the electrostatic interaction but also facilitate the interactions with the hydrophobic surface of the protein, such as Lys53, Glu71, Met109, Thr106, and Asp168. The salt bridge between Lys53 and Glu71 is important to stabilize the conformations of the side chains of the two residues, maintaining their hydrophobic interactions with inhibitors. The findings in this work could provide a better structural understanding of allosteric inhibitors targeting the DFG-out form of protein kinase and a basis for further rational design of new potent inhibitors to p38.

AUTHOR INFORMATION

Corresponding Author

*E-mail: xjyao@lzu.edu.cn. Telephone: +86-931-891-2578.

ACKNOWLEDGMENT

This work was supported by the Program for New Century Excellent Talents in University (grant no. NCET-07-0399), the National Natural Science Foundation of China (grant no. 20905033), and the Fundamental Research Funds for the Central Universities (grant no. lzujbky-2011-19).

REFERENCES

- Cuenda, A.; Rousseau, S. p38 MAP-Kinases pathway regulation, function and role in human diseases. *Biochim. Biophys. Acta* **2007**, *1773*, 1358–1375.
- Kumar, S.; Boehm, J.; Lee, J. C. p38 MAP kinases: key signalling molecules as therapeutic targets for inflammatory diseases. *Nat. Rev. Drug Discovery* **2003**, *2*, 717–726.
- Peifer, C.; Wagner, G.; Laufer, S. New approaches to the treatment of inflammatory disorders small molecule inhibitors of p38 MAP kinase. *Curr. Top. Med. Chem.* **2006**, *6*, 113–149.
- Schindler, J.; Monahan, J.; Smith, W. p38 pathway kinases as anti-inflammatory drug targets. *J. Dent. Res.* **2007**, *86*, 800–811.
- Dominguez, C.; Powers, D.; Tamayo, N. p38 MAP kinase inhibitors: many are made, but few are chosen. *Curr. Opin. Drug Discovery Dev.* **2005**, *8*, 421–430.
- Lee, M. R.; Dominguez, C. MAP Kinase p38 Inhibitors: Clinical Results and an Intimate Look at Their Interactions with p38alpha Protein. *Curr. Med. Chem.* **2005**, *12*, 2979–2994.
- Pettus, L. H.; Wurz, R. P. Small molecule p38 MAP kinase inhibitors for the treatment of inflammatory diseases: novel structures and developments during 2006–2008. *Curr. Top. Med. Chem.* **2008**, *8*, 1452–1467.
- Liu, Y.; Gray, N. S. Rational design of inhibitors that bind to inactive kinase conformations. *Nat. Chem. Biol.* **2006**, *2*, 358–364.
- Zhang, J.; Adrián, F. J.; Jahnke, W.; Cowan-Jacob, S. W.; Li, A. G.; Jacob, R. E.; Sim, T.; Powers, J.; Dierks, C.; Sun, F. Targeting Bcr–Abl by combining allosteric with ATP-binding-site inhibitors. *Nature* **2010**, *463*, 501–506.
- García-Echeverría, C. Allosteric and ATP-competitive kinase inhibitors of mTOR for cancer treatment. *Bioorg. Med. Chem. Lett.* **2010**, *20*, 4308–4312.
- Dietrich, J.; Hulme, C.; Hurley, L. H. The design, synthesis, and evaluation of 8 hybrid DFG-out allosteric kinase inhibitors: A structural analysis of the binding interactions of Gleevec®, Nexavar®, and BIRB-796. *Bioorg. Med. Chem.* **2010**, *18*, 5738–5748.
- Simard, J. R.; Pawar, V.; Aust, B.; Wolf, A.; Rabiller, M.; Wulfert, S.; Robubi, A.; Klu ter, S.; Ottmann, C.; Rauh, D. High-Throughput Screening To Identify Inhibitors Which Stabilize Inactive Kinase Conformations in p38. *J. Am. Chem. Soc.* **2009**, *131*, 18478–18488.
- Simard, J. R.; Klüter, S.; Grütter, C.; Getlik, M.; Rabiller, M.; Rode, H. B.; Rauh, D. A new screening assay for allosteric inhibitors of cSrc. *Nat. Chem. Biol.* **2009**, *5*, 394–396.
- Simard, J. R.; Getlik, M.; Grütter, C.; Pawar, V.; Wulfert, S.; Rabiller, M.; Rauh, D. Development of a fluorescent-tagged kinase assay system for the detection and characterization of allosteric kinase inhibitors. *J. Am. Chem. Soc.* **2009**, *131*, 13286–13296.
- Jacobs, M. D.; Caron, P. R.; Hare, B. J. Classifying protein kinase structures guides use of ligand selectivity profiles to predict inactive conformations: Structure of lck/imatinib complex. *Proteins: Struct. Funct. Bioinform.* **2008**, *70*, 1451–1460.
- Pargellis, C.; Tong, L.; Churchill, L.; Cirillo, P. F.; Gilmore, T.; Graham, A. G.; Grob, P. M.; Hickey, E. R.; Moss, N.; Pav, S. Inhibition of p38 MAP kinase by utilizing a novel allosteric binding site. *Nat. Struct. Mol. Biol.* **2002**, *9*, 268–272.
- Backes, A.; Zech, B.; Felber, B.; Klebl, B.; Müller, G. Small-molecule inhibitors binding to protein kinase. Part II: the novel pharmacophore approach of type II and type III inhibition. *Expert Opin. Drug Discovery* **2008**, *3*, 1427–1449.
- Kufareva, I.; Abagyan, R. Type-II kinase inhibitor docking, screening, and profiling using modified structures of active kinase states. *J. Med. Chem.* **2008**, *51*, 7921–7932.
- Liao, J. J.-L.; Robert, A. C. Targeting protein multiple conformations: a structure-based strategy for kinase drug design. *Curr. Top. Med. Chem.* **2007**, *7*, 1394–1407.
- Capdeville, R.; Buchdunger, E.; Zimmermann, J.; Matter, A. Glivec (ST1571, imatinib), a rationally developed, targeted anticancer drug. *Nat. Rev. Drug Discovery* **2002**, *1*, 493–502.

- (21) Deininger, M.; Buchdunger, E.; Druker, B. J. The development of imatinib as a therapeutic agent for chronic myeloid leukemia. *Blood* **2005**, *105*, 2640–2653.
- (22) Wilhelm, S.; Carter, C.; Lynch, M.; Lowinger, T.; Dumas, J.; Smith, R. A.; Schwartz, B.; Simantov, R.; Kelley, S. Discovery and development of sorafenib: a multikinase inhibitor for treating cancer. *Nat. Rev. Drug Discovery* **2006**, *5*, 835–844.
- (23) Branger, J.; van den Blink, B.; Weijer, S.; Madwed, J.; Bos, C. L.; Gupta, A.; Yong, C. L.; Polmar, S. H.; Olszyna, D. P.; Hack, C. E. Anti-inflammatory effects of a p38 mitogen-activated protein kinase inhibitor during human endotoxemia. *J. Immunol.* **2002**, *168*, 4070–4077.
- (24) Regan, J.; Capolino, A.; Cirillo, P. F.; Gilmore, T.; Graham, A. G.; Hickey, E.; Kroe, R. R.; Madwed, J.; Moriak, M.; Nelson, R. Structure-Activity Relationships of the p38 MAP Kinase Inhibitor 1-(5-tert-Butyl-2-p-tolyl-2 H-pyrazol-3-yl)-3-[4-(2-morpholin-4-yl-ethoxy)naphthalen-1-yl] urea (BIRB 796). *J. Med. Chem.* **2003**, *46*, 4676–4686.
- (25) Namboodiri, H. V.; Bukhtiyarova, M.; Ramcharan, J.; Karpusas, M.; Lee, Y.; Springman, E. B. Analysis of imatinib and sorafenib Binding to p38α Compared with c-Abl and b-Raf Provides Structural Insights for Understanding the Selectivity of Inhibitors Targeting the DFG-Out Form of Protein Kinases. *Biochemistry* **2010**, *49*, 3611–3618.
- (26) Karcher, S. C.; Laufer, S. A. Successful structure-based design of recent p38 MAP kinase inhibitors. *Curr. Top. Med. Chem.* **2009**, *9*, 655–676.
- (27) Hynes, J.; Leftheris, K. Small molecule p38 inhibitors: novel structural features and advances from 2002–2005. *Curr. Top. Med. Chem.* **2005**, *5*, 967–985.
- (28) Xiao, Z.; Varma, S.; Xiao, Y. D.; Tropsha, A. Modeling of p38 mitogen-activated protein kinase inhibitors using the Catalyst (TM) HypoGen and k-nearest neighbor QSAR methods. *J. Mol. Graphics Modell.* **2004**, *23*, 129–138.
- (29) Romeiro, N. C.; Albuquerque, M. G.; Alencastro, R. B.; Ravi, M.; Hopfinger, A. J. Construction of 4D-QSAR models for use in the design of novel p38-MAPK inhibitors. *J. Comput.-Aided Mol. Des.* **2005**, *19*, 385–400.
- (30) Ravindra, G.; Achaiah, G.; Sastry, G. Molecular modeling studies of phenoxypyrimidinyl imidazoles as p38 kinase inhibitors using QSAR and docking. *Eur. J. Med. Chem.* **2008**, *43*, 830–838.
- (31) Shah, U. A.; Deokar, H. S.; Kadam, S. S.; Kulkarni, V. M. 3D-QSAR and pharmacophore identification of novel imidazolyl benzimidazoles and imidazo [4, 5-b] pyridines as potent p38 mitogen activated protein kinase inhibitors. *Int. J. ChemTech Res.* **2010**, *2*, 194–204.
- (32) Sarma, R.; Sinha, S.; Ravikumar, M.; Kishore Kumar, M.; Mahmood, S. Pharmacophore modeling of diverse classes of p38 MAP kinase inhibitors. *Eur. J. Med. Chem.* **2008**, *43*, 2870–2876.
- (33) Cheeseright, T. J.; Holm, M.; Lehmann, F.; Luik, S.; Go ttet, M.; Melville, J. L.; Laufer, S. Novel lead structures for p38 MAP kinase via FieldScreen virtual screening. *J. Med. Chem.* **2009**, *52*, 4200–4209.
- (34) Gill, A. L.; Frederickson, M.; Cleasby, A.; Woodhead, S. J.; Carr, M. G.; Woodhead, A. J.; Walker, M. T.; Congreve, M. S.; Devine, L. A.; Tisi, D. Identification of novel p38α MAP kinase inhibitors using fragment-based lead generation. *J. Med. Chem.* **2005**, *48*, 414–426.
- (35) Chen, J.; Zhang, Z.; Stebbins, J. L.; Zhang, X.; Hoffman, R.; Moore, A.; Pellecchia, M. A Fragment-Based Approach for the Discovery of Isoform-Specific p38 Inhibitors. *ACS Chem. Biol.* **2007**, *2*, 329–336.
- (36) Frembgen-Kesner, T.; Elcock, A. H. Computational sampling of a cryptic drug binding site in a protein receptor: explicit solvent molecular dynamics and inhibitor docking to p38 MAP kinase. *J. Mol. Biol.* **2006**, *359*, 202–214.
- (37) Filomia, F.; De Rienzo, F.; Menziani, M. C. Insights into mapk p38α DFG flip mechanism by accelerated molecular dynamics. *Bioorg. Med. Chem.* **2010**, *18*, 6805–6812.
- (38) Pearlman, D. A.; Charifson, P. S. Are free energy calculations useful in practice? A comparison with rapid scoring functions for the p38 MAP kinase protein system. *J. Med. Chem.* **2001**, *44*, 3417–3423.
- (39) Pearlman, D. A. Evaluating the molecular mechanics Poisson-Boltzmann surface area free energy method using a congeneric series of ligands to p38 MAP kinase. *J. Med. Chem.* **2005**, *48*, 7796–7807.
- (40) Luccarelli, J.; Michel, J.; Tirado-Rives, J.; Jorgensen, W. L. Effects of Water Placement on Predictions of Binding Affinities for p38 MAP Kinase Inhibitors. *J. Chem. Theory Comput.* **2010**, *6*, 3850–3856.
- (41) Badrinarayanan, P.; Sastry, G. N. Sequence, Structure, and Active Site Analyses of p38 MAP Kinase: Exploiting DFG-out Conformation as a Strategy to Design New Type II Leads. *J. Chem. Inf. Model.* **2010**, *51*, 115–129.
- (42) Chen, Q.; Cui, W.; Ji, M. Studies of chirality effect of 4-(phenylamino)-pyrrolo [2, 1-f][1, 2, 4] triazine on p38 by molecular dynamics simulations and free energy calculations. *J. Comput.-Aided Mol. Des.* **2009**, *23*, 737–745.
- (43) Alonso, H.; Bliznyuk, A. A.; Gready, J. E. Combining docking and molecular dynamic simulations in drug design. *Med. Res. Rev.* **2006**, *26*, 531–568.
- (44) Kollman, P. A.; Massova, I.; Reyes, C.; Kuhn, B.; Huo, S.; Chong, L.; Lee, M.; Lee, T.; Duan, Y.; Wang, W.; Donini, O.; Cieplak, P.; Srinivasan, J.; Case, D. A.; Cheatham, T. E. Calculating structures and free energies of complex molecules: combining molecular mechanics and continuum models. *Acc. Chem. Res.* **2000**, *33*, 889–897.
- (45) Gohlike, H.; Kiel, C.; Case, D. A. Insights into protein–protein binding by binding free energy calculation and free energy decomposition for the Ras-Raf and Ras-RalGDS complexes. *J. Mol. Biol.* **2003**, *330*, 891–913.
- (46) Massova, I.; Kollman, P. A. Combined molecular mechanical and continuum solvent approach (MM-PBSA/GBSA) to predict ligand binding. *Perspect. Drug Discovery* **2000**, *18*, 113–135.
- (47) Rastelli, G.; Rio, A. D.; Degliesposti, G.; Sgobba, M. Fast and accurate predictions of binding free energies using MM-PBSA and MM-GBSA. *J. Comput. Chem.* **2010**, *31*, 797–810.
- (48) Gohlike, H.; Case, D. A. Converging free energy estimates: MM-PB(GB)SA studies on the protein–protein complex Ras–Raf. *J. Comput. Chem.* **2004**, *25*, 238–250.
- (49) Wang, J.; Morin, P.; Wang, W.; Kollman, P. A. Use of MM-PBSA in reproducing the binding free energies to HIV-1 RT of TIBO derivatives and predicting the binding mode to HIV-1 RT of efavirenz by docking and MM-PBSA. *J. Am. Chem. Soc.* **2001**, *123*, 5221–5230.
- (50) Hou, T.; Guo, S.; Xu, X. Predictions of binding of a diverse set of ligands to gelatinase-A by a combination of molecular dynamics and continuum solvent models. *J. Phys. Chem. B* **2002**, *106*, 5527–5535.
- (51) Huo, S.; Wang, J.; Cieplak, P.; Kollman, P. A.; Kuntz, I. D. Molecular dynamics and free energy analyses of cathepsin D-inhibitor interactions: insight into structure-based ligand design. *J. Med. Chem.* **2002**, *45*, 1412–1419.
- (52) Hou, T.; Chen, K.; McLaughlin, W. A.; Lu, B.; Wang, W. Computational analysis and prediction of the binding motif and protein interacting partners of the Abl SH3 domain. *PLoS Comput. Biol.* **2006**, *2*, 0046–0055.
- (53) Hou, T.; McLaughlin, W.; Lu, B.; Chen, K.; Wang, W. Prediction of binding affinities between the human amphiphysin-1 SH3 domain and its peptide ligands using homology modeling, molecular dynamics and molecular field analysis. *J. Proteome Res.* **2006**, *5*, 32–43.
- (54) Weis, A.; Katebzadeh, K.; Söderhjelm, P.; Nilsson, I.; Ryde, U. Ligand affinities predicted with the MM/PBSA method: dependence on the simulation method and the force field. *J. Med. Chem.* **2006**, *49*, 6596–6606.
- (55) Hou, T.; McLaughlin, W. A.; Wang, W. Evaluating the potency of HIV 1 protease drugs to combat resistance. *Proteins: Struct., Funct., Bioinform.* **2008**, *71*, 1163–1174.
- (56) Hou, T.; Zhang, W.; Case, D. A.; Wang, W. Characterization of Domain–Peptide Interaction Interface: A Case Study on the Amphiphysin-1 SH3 Domain. *J. Mol. Biol.* **2008**, *376*, 1201–1214.
- (57) Stoica, I.; Sadiq, S. K.; Coveney, P. V. Rapid and accurate prediction of binding free energies for saquinavir-bound HIV-1 proteases. *J. Am. Chem. Soc.* **2008**, *130*, 2639–2648.
- (58) Zeng, J.; Li, W.; Zhao, Y.; Liu, G.; Tang, Y.; Jiang, H. Insights into ligand selectivity in estrogen receptor isoforms: molecular dynamics simulations and binding free energy calculations. *J. Phys. Chem. B* **2008**, *112*, 2719–2726.

- (59) Hou, T.; Xu, Z.; Zhang, W.; McLaughlin, W. A.; Case, D. A.; Xu, Y.; Wang, W. Characterization of Domain-Peptide Interaction Interface. *Mol. Cell. Proteomics* **2009**, *8*, 639–649.
- (60) Thompson, D. C.; Humblet, C.; Joseph-McCarthy, D. Investigation of MM-PBSA rescoring of docking poses. *J. Chem. Inf. Model.* **2008**, *48*, 1081–1091.
- (61) Guimaraes, C. R. W.; Cardozo, M. MM-GB/SA rescoring of docking poses in structure-based lead optimization. *J. Chem. Inf. Model.* **2008**, *48*, 958–970.
- (62) Kuhn, B.; Gerber, P.; Schulz-Gasch, T.; Stahl, M. Validation and use of the MM-PBSA approach for drug discovery. *J. Med. Chem.* **2005**, *48*, 4040–4048.
- (63) Gennheden, S.; Ryde, U. How to obtain statistically converged MM/GBSA results. *J. Comput. Chem.* **2010**, *31*, 837–846.
- (64) Zoete, V.; Michielin, O. Comparison between computational alanine scanning and per residue binding free energy decomposition for protein–protein association using MM GBSA: Application to the TCR p-MHC complex. *Proteins: Struct., Funct., Bioinform.* **2007**, *67*, 1026–1047.
- (65) *Discovery Studio*, version 2.5.5; Accelrys, Inc.: San Diego, CA, 2010.
- (66) *Maestro*, version 9.0; Schrödinger, LLC: New York, NY, 2009.
- (67) *Prime*, version 2.0; Schrödinger, LLC: New York, NY, 2008.
- (68) *Impact*, version 5.0; Schrödinger, LLC: New York, NY, 2005.
- (69) *QSite*, version 5.5; Schrödinger, LLC: New York, NY, 2009.
- (70) Wang, J.; Wolf, R. M.; Caldwell, J. W.; Kollman, P. A.; Case, D. A. Development and testing of a general amber force field. *J. Comput. Chem.* **2004**, *25*, 1157–1174.
- (71) Duan, Y.; Wu, C.; Chowdhury, S.; Lee, M. C.; Xiong, G.; Zhang, W.; Yang, R.; Cieplak, P.; Luo, R.; Lee, T.; Caldwell, J.; Wang, J.; Kollman, P. A point-charge force field for molecular mechanics simulations of proteins based on condensed-phase quantum mechanical calculations. *J. Comput. Chem.* **2003**, *24*, 1999–2012.
- (72) Jorgensen, W.; Chandrasekhar, J.; Madura, J.; Impey, R.; Klein, M. Comparison of simple potential functions for simulating liquid water. *J. Chem. Phys.* **1983**, *79*, 926–935.
- (73) Case, D. A.; Cheatham, T. E., III; Darden, T.; Gohlke, H.; Luo, R.; Merz, K. M., Jr.; Onufriev, A.; Simmerling, C.; Wang, B.; Woods, R. J. The Amber biomolecular simulation programs. *J. Comput. Chem.* **2005**, *26*, 1668–1688.
- (74) Berendsen, H. J. C.; Postma, J. P. M.; Vangunsteren, W. F.; Dinola, A.; JR, H. Molecular-dynamics with coupling to an external bath. *J. Chem. Phys.* **1984**, *81*, 3684–3690.
- (75) Darden, T.; York, D.; Pedersen, L. Particle mesh Ewald: An N·log(N) method for Ewald sums in large systems. *J. Chem. Phys.* **1993**, *98*, 10089–10092.
- (76) Ryckaert, J.; Ciccotti, G.; Berendsen, H. Numerical integration of the cartesian equations of motion of a system with constraints: molecular dynamics of n-alkanes. *J. Comput. Phys.* **1977**, *23*, 327–341.
- (77) Rocchia, W.; Alexov, E.; Honig, B. Extending the applicability of the nonlinear Poisson-Boltzmann equation: Multiple dielectric constants and multivalent ions. *J. Phys. Chem. B* **2001**, *105*, 6507–6514.
- (78) Onufriev, A.; Bashford, D.; Case, D. A. Exploring protein native states and large-scale conformational changes with a modified generalized born model. *Proteins: Struct., Funct., Bioinform.* **2004**, *55*, 383–394.
- (79) Wlodek, S. T.; Clark, T. W.; Scott, L. R.; McCammon, J. A. Molecular dynamics of acetylcholinesterase dimer complexed with tacrine. *J. Am. Chem. Soc.* **1997**, *119*, 9513–9522.